This article has been accepted for publication in a future issue of this journal, but has not been fully edited. Content may change prior to final publication. Citation information: DOI 10.1109/ACCESS.2021.3079204, IEEE Access

IEEE Access
Multidisciplinary | Rapid Review | Open Access Journal

Date of publication xxxx 00, 0000, date of current version xxxx 00, 0000.

Digital Object Identifier 10.1109/ACCESS.2017.DOI

A Novel Deep-Learning Model for Automatic Detection and Classification of Breast Cancer Using the Transfer-Learning Technique

ABEER SABER[1], MOHAMED SAKR[2], OSAMA M. ABO-SEIDA[1], ARABI KESHK[2], and HUILING CHEN*[3]

[1]Department of Computer Science, Faculty of Computers and Information, Kafr El-Sheikh University, Kafr El-Sheikh 33511, Egypt.
Abeer_Saber@fci.kfs.edu.eg, aboseida@yahoo.com
[2]Department of Computer Science, Faculty of Computers and Information, Menoufia University, Menoufia 32511, Egypt.
mohamed.sakr@ci.menofia.edu.eg, arabi.keshk@ci.menofia.edu.eg
[3]Department of Computer Science and Artificial Intelligence, Wenzhou University, Wenzhou 325035, China

Corresponding author: Huiling Chen (chenhuiling.jlu@gmail.com).

ABSTRACT Breast cancer (BC) is one of the primary causes of cancer death among women. Early detection of BC allows patients to receive appropriate treatment, thus increasing the possibility of survival. In this work, a new deep-learning (DL) model based on the transfer-learning (TL) technique is developed to efficiently assist in the automatic detection and diagnosis of the BC suspected area based on two techniques namely 80-20 and cross-validation. DL architectures are modeled to be problem-specific. TL uses the knowledge gained during solving one problem in another relevant problem. In the proposed model, the features are extracted from the mammographic image analysis- society (MIAS) dataset using a pre-trained convolutional neural network (CNN) architecture such as Inception V3, ResNet50, Visual Geometry Group networks (VGG)-19, VGG-16, and Inception-V2 ResNet. Six evaluation metrics for evaluating the performance of the proposed model in terms of accuracy, sensitivity, specificity, precision, F-score, and area under the ROC curve (AUC) has been chosen. Experimental results show that the TL of the VGG16 model is powerful for BC diagnosis by classifying the mammogram breast images with overall accuracy, sensitivity, specificity, precision, F-score, and AUC of 98.96%, 97.83%, 99.13%, 97.35%, 97.66%, and 0.995, respectively for 80-20 method and 98.87%, 97.27%, 98.2%, 98.84%, 98.04%, and 0.993 for 10-fold cross-validation method.

INDEX TERMS Breast Cancer; Machine Learning, Deep-Learning, Transfer Learning, Image Classification, Convolutional Neural Networks.

I. INTRODUCTION

Cancer tumor is related to abnormal cell growth, which invades the surrounding tissues in the human body. There are two types of tumor: benign and malignant. A benign tumor consists of non–cancerous cells that grow only locally and do not spread in the human body. in contrast, a malignant tumor consists of cancerous cells, which are capable of multiplying uncontrollably, spreading to various parts of the human body, and invading the tissues. In the USA, approximately 12% of women are expected to be diagnosed with BC over their lifetime. On average, one woman every two minutes is diagnosed with BC in the USA [1], [2]. This makes BC the most common type of cancer in women [3]. BC is a disease in which breast cells grow uncontrollably. The BC type depends on the cells that become cancerous. BC can start in various parts of the breast. Breast consists of three main parts: lobes, ducts, and connective tissue. Most BCs start in the ducts or lobules. Therefore, early BC detection is significant in increasing patient survival rates. The high morbidity and considerable cost of healthcare-associated with cancer have instigated researchers to implement more precise models for cancer detection. Mammography and biopsy are the two most common methodologies for BC detection. In mammography, radiologist uses a specific type of breast images to detect

This article has been accepted for publication in a future issue of this journal, but has not been fully edited. Content may change prior to final publication. Citation information: DOI 10.1109/ACCESS.2021.3079204, IEEE Access

early symptoms of cancer in women. Studies have shown that mammography has led to a reduction in death rates caused by BC. A biopsy is another efficient diagnostic methodology for BC detection. Automatic identification and localization of cancer cells are the main challenges in BC images due to their variance in size, shape, and location. Other abnormalities, such as mastitis, adenopathy, and granuloma, may also be found in breast images [4]. Machine learning (ML) techniques have found its wide applications in many fields such as prediction problems in educational field [5]–[9], bankruptcy prediction [10]–[16], pattern recognition [17]–[28], image editing [29]–[39], feature reduction [40]–[44], fault diagnosis [45]–[50], face recognition and micro-expression recognition [51]–[57], natural language processing [58], [59] and medical diagnosis [60]–[74]. Especially, it has found its great potential in BC diagnosis. In recent decades, various solutions for automatic cell classification in BC detection have been suggested by many researchers. In this context, some researchers have worked on nucleus analysis by extracting nucleus features that represent useful information in classifying cells into benign or malignant [75]. Similarly, grouping-based algorithms using the circular Hough-transform and various statistical features have also been exploited for nuclei segmentation and classification. However, due to the complex nature of classic ML techniques, such as preprocessing, segmentation, feature extraction, and other, the system's performance degrades in terms of efficiency and accuracy. Traditional ML challenges can be overcome by the DL method, which has emerged recently. This method is capable of achieving outstanding feature representation to solve image-classification and object-localization tasks. The most popular of the DL algorithms proposed in the literature are the CNNs. The CNN architecture is specially modified with the 2D input-image structure [76], [77]. A CNN-training task requires a large amount of data, which lack in the medical domain, especially in BC. A solution to this problem is to use the TL technique from a natural-images dataset, such as ImageNet, and implement a fine-tuning technique, as shown in Fig. 1. The TL concept can be exploited to enhance the performance of individual CNN architectures by combining their knowledge [78]. The major advantage of TL is the enhancement of classification accuracy and the speed-up of the training process. An appropriate TL method is a model transfer; first, the network parameters are pre-trained using the source data, then these parameters are applied in the target domain, and finally the network parameters are adjusted for better performance [79]. In this context, a framework for multi-class BC detection and classification based on TL is proposed and implemented. The proposed model consists of two main components. The first component consists of six main phases (noise removal, histogram equalization, morphological analysis, segmentation, image resizing, data splitting, and data augmentation), which are applied to improve the breast images. Then, a pre-trained CNN such as, the Inception V3, VGG19, VGG16, ResNet50, and Inception-V2 ResNet, are used to transfer their learned parameters to the BC-classification task. The major objectives of this work are the automatic extraction of the affected patch using segmentation, reduction in training time, and improvement in classification performance.

This paper has the following contributions:

1) Reducing training time by extracting only the affected regions from breast images.

2) Using noise reduction, histogram equalization, and morphological analysis methods to improve the affected areas detection.

3) Improving the classification performance by changing the pre-trained networks classifier.

4) Solving the problem of overfitting.

Other contributions of this paper as follows:

- DL is introduced to help in BC automatic diagnosis.
- Compared between many pre-trained CNN such as Inception V3, ResNet50, VGG-16, VGG-19, and Inception-V2 ResNet results.
- Six different measures are used as accuracy, sensitivity, specifity, precision, AUC, and F-score.

This paper is organized as follows. In Section II, the related work is discussed, whereas a description of the proposed model for BC detection and classification using TL techniques is presented in Section III. The experimental results compared with real data are presented in Section IV. Finally, the paper is concluded in Section V.

II. RELATED WORK

Ting et al. [80] implemented a deep CNN for BC-lesion classification. This network consisted of 1 input layer, 28 hidden layer, and 1 output layer. Overfitting was avoided using the feature-wise-data augmentation (FWDA) algorithm. Their proposed method sequentially achieved 89.47%, 90.50%, and 90.71% for sensitivity, accuracy, and specificity, respectively. Toğaçar et al. [81] proposed the BreastNet, which consisted of convolutional, pooling, residual, and dense blocks, and it was capable of extracting the most effective features from breast images. BreastNet achieved better results than AlexNet, VGG-16, and VGG-19 models as its accuracy approached 98.80%. Abbas [82] presented a multi-layer DL architecture for classifying benign and malignant regions in breast images. This network consisted of four phases for extracting invariant features, which were transformed into deep-invariant features, and learning features for making the final decision. In [82], the MIAS dataset was used and achieved a 92%, 84.2%, 91.5%, and 0.91 for sensitivity, specificity, accuracy, and AUC, respectively. Using the same dataset, Sha et al. [83] presented a method for automatic detection and classification of the cancerous region in breast images. Their proposed method was based on CNNs and the grasshopper optimization algorithm. The results showed that this proposed method was capable of achieving 96%, 93%, and 92% for sensitivity, specificity, and accuracy, respectively. Charan et al. [84] trained a CNN for BC detection. Their proposed CNN consisted of six convolution layers, four average-pooling layers, and three fully-connected layers

This article has been accepted for publication in a future issue of this journal, but has not been fully edited. Content may change prior to final publication. Citation information: DOI 10.1109/ACCESS.2021.3079204, IEEE Access

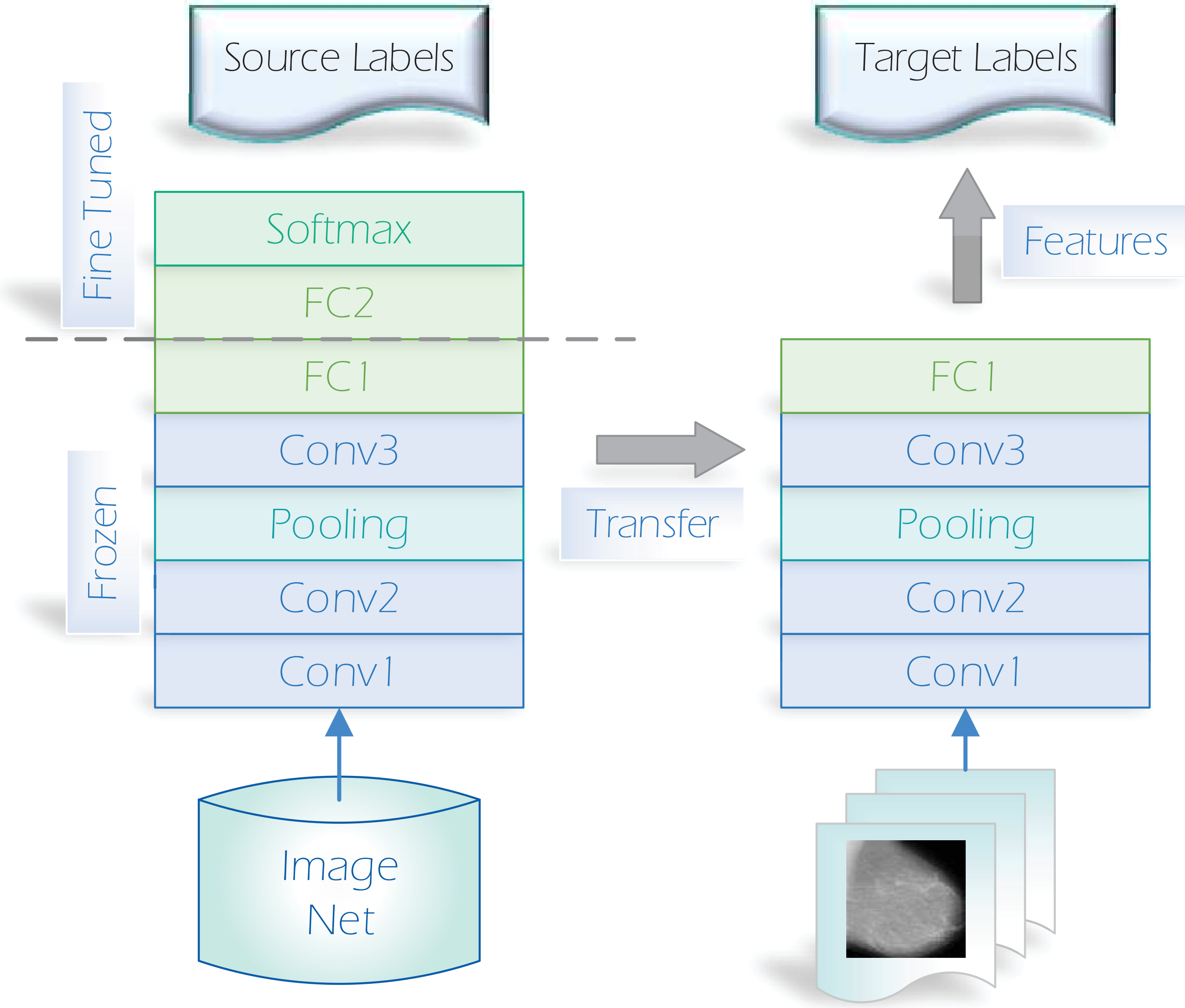

FIGURE 1: Transfer learning method

(FCLs). They used a size of 224 x 224 for the input image and the Softmax (SM) function to apply the classification results. The overall accuracy of this network was 65%, which was obtained using the MIAS database. In [85], Wahab et al. exploited a pre-trained CNN and transferred its learned parameters to another CNN for mitoses classification. Their proposed method achieved 0.50, 0.80, and 0.621 for precision, recall, and F-measure, respectively. In addition, for multi-class BC-classification purposes, Lotter et al. [75] proposed a model in which the features were extracted using a pre-trained ResNet50 network. Their model was capable of classifying lesions into five classes: mass, calcifications, focal asymmetry, architectural distortion, or no lesion. Their model achieved 96.2, 90.9, and 0.94 for sensitivity, specificity, and AUC, respectively. Jiang et al. [86] achieved better BC-classification accuracy in the case of TL from a pre-trained network in building networks from scratch. The accuracy approached 0.88 using GoogleNet and 0.83 using AlexNet on the film mammography number 3 (BCDR-F03) dataset. Khan et al. [87] implemented a model in which the breast-image features were extracted using pre-trained CNN architectures, namely, GoogleNet, VGGNet, and ResNet. The model's accuracy, which approached 97.525%, was evaluated using a standard benchmark dataset. Cao et al. [88] improved the performance of TL for BC-classification without any fine-tuning on the source network layers (ResNet-125). Instead, they used random forest dissimilarity for combining various feature groups. The "ICIAR 2018" dataset was used, and the classification accuracy was improved to 82.90%. Deniz et al. [89] fine-tuned the last three layers in the AlexNet and VGG16 models to classify breast tumors on the BreaKHis dataset. Their model achieved better accuracy than five other

This article has been accepted for publication in a future issue of this journal, but has not been fully edited. Content may change prior to final publication. Citation information: DOI 10.1109/ACCESS.2021.3079204, IEEE Access

methods as it approached 91.37%. In the same dataset, Celik et al. [90] pre-trained the DenseNet-161 model and achieved 92.38% and 91.57% for the F-score and accuracy, respectively.

III. MATERIALS AND METHODS

The proposed method for BC detection and classification consists of two main components. The first component is used for data preprocessing and the second for transferring the CNN parameters, as shown in Figs. 2 and 3.

A. DATA PREPROCESSING

Image preprocessing is very important to remove the limits of observing abnormalities without undue influence from a mammogram. In this work, the tumor regions are automatically extracted using segmentation techniques before the learning process to reduce computation time. Image quality can be improved and the segmentation results can become more accurate using noise removal, histogram equalization, and morphological analysis before segmentation. As shown in Fig. 2, data preprocessing consists of seven phases.

1) Noise removal

A 2D median filter of a 3 x 3 size is applied to remove the digitization noise from the mammogram image.

2) Histogram equalization

Classical histogram equalization is applied to improve the contrast for all levels of the original image. This is accomplished by effectively distributing the most frequent gray level of the image that is, stretching the intensity range of the image. In mammogram images, histogram equalization is applied to make contrast adjustment so that image anomalies become more visible.

3) Morphological analysis

The morphological analysis is an important process for removing non-breast regions before segmentation so that the results are not affected. In morphological operations, the relevant structures are extracted from the input image after applying the structuring element (SE). The output image of this operation has the size of the input. The value of each pixel depends on the corresponding pixel in the input and its neighbors. The operations described in Fig. 4 can be estimated as follows [91]:

- Image Opening (IO)

$$\mathrm{IO} = \mathrm{Inp} \ominus \mathrm{SE} \oplus \mathrm{SE} \tag{1}$$

- Image Closing (IC)

$$\mathrm{IC} = \mathrm{Inp} \oplus \mathrm{SE} \ominus \mathrm{SE} \tag{2}$$

- White Top-hat (WTH)

$$\mathrm{WTH} = \mathrm{Inp} - \mathrm{IO} \tag{3}$$

- Black Top-hat (BTH)

$$\mathrm{BTH} = \mathrm{IC} - \mathrm{Inp} \tag{4}$$

- Mathematical Morphological (MM)

$$\mathrm{MM} = \mathrm{Inp} + \mathrm{WTH} - \mathrm{BTH} \tag{5}$$

where $\oplus$ and $\ominus$ refer to the dilation and erosion operations, respectively.

4) Segmentation

The computation time can be reduced, and the analysis can be focused on the region mostly affected by cancer using a threshold-based segmentation method for automatic patch extraction [92].

5) Image resizing

The breast images are resized and converted into three channels: red green, and blue (RGB) to match the input size of the pretrained CNN architecture.

6) Data splitting

The MIAS dataset is split into "80%" for the training set and "20%" for the testing set [93]–[95].
In addition, to overcome the problem of over-fitting, the experiments have been re-performed using a cross-validation technique with 10-folds. The cross-validation idea is the partitioning of the dataset to k folds with equal size. After that, k-1 folds will be used to train the classifier and the remaining fold will be used to test data to predict each sample label. The final result is the average of different data rounds [96].

7) Data augmentation algorithm (DDA)

DL models work better when large datasets are used. Data augmentation is considered one of the most popular methods to increase the size of the dataset, which helps overcome overfitting when training a very small amount of data. In this work, the training data can be augmented using a set of transformations. DAA is implemented to increase the input data. First, the segmented images are rotated clockwise to 90º, 180º, 270º, and 360º. Then, every rotated image is flipped vertically. In this way, an input image will produce eight images. The detailed algorithm for data augmentation is shown in Alg. 1.

B. DEEP-CNN TRAINING BASED ON TL

In this work, the Inception V3, ResNet50, VGG19, VGG16, and Inception-V2 ResNet networks are used for feature extraction. These networks are trained using the ImageNet dataset. The filters in the network layers are used to recognize the input features such as colors, vertical, and horizontal lines. Subsequently, trivial shapes and small parts can be recognized. From the generated output, the class in which the input image belongs (i.e. cats, birds, and other) can be determined. Next, the pre-trained network for classifying

This article has been accepted for publication in a future issue of this journal, but has not been fully edited. Content may change prior to final publication. Citation information: DOI 10.1109/ACCESS.2021.3079204, IEEE Access

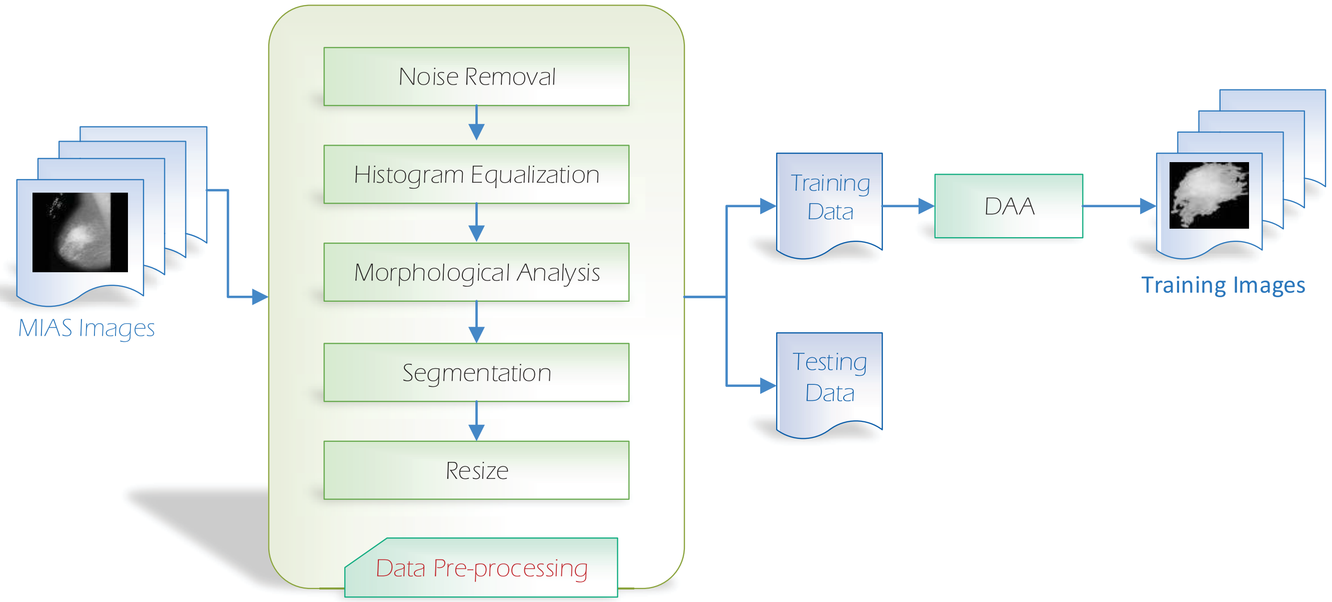

FIGURE 2: Data pre-processing

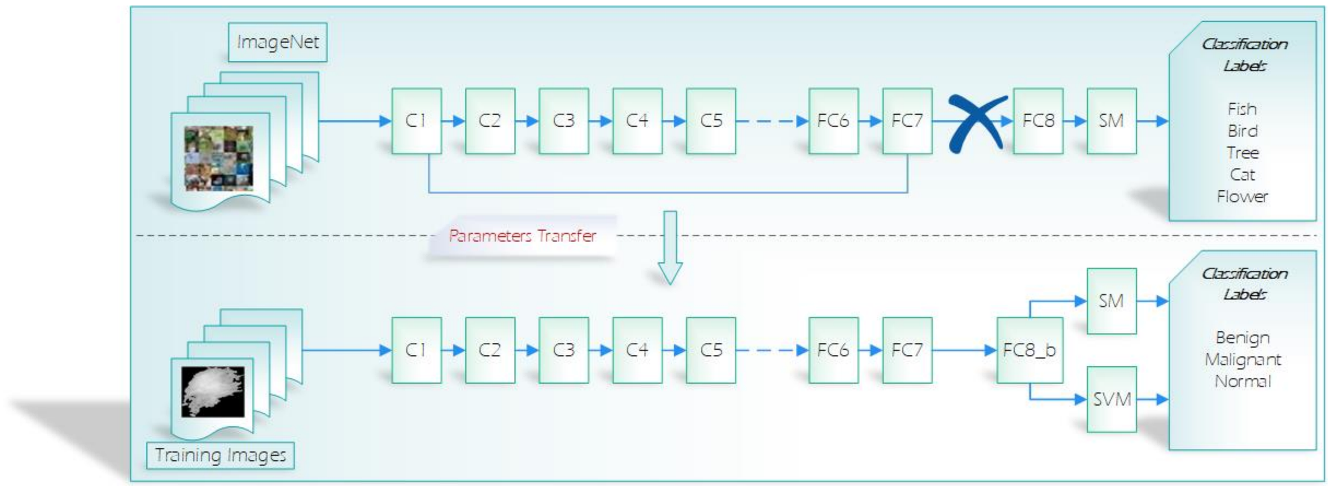

FIGURE 3: Transferring CNN parameters

different objects in a new dataset is applied (in this work for BC-classification to perform TL). The trained parameters from the source task, except for the last three (FCL, SM, and classification) layers are frozen and transferred to the target task, as shown in Fig. 3. Then, the extracted patches from the segmentation process during preprocessing are used to continue the network training. Hence, the newly-trained dense layers are few. Furthermore, the already-trained layers in the pre-trained network are combined with these layers for a new class classification. Thus, the training process can be created very quickly and very few training data are needed compared with the CNN training from scratch. The extracted features are then used to train support vector machine (SVM) and SM classifiers for applying classification task. Fine-tuning is conducted using the stochastic gradient-descent (SGD) method with momentum (SGDM), which is actually an improved version of SGD with the learning parameters shown in Table 1. SGDM' goal is to increase velocity in all dimensions, even in those with consistent gradient. Due to SGDM jittering, gradient high-velocity dimensions are reduced, whereas past gradients that have some momentum are reduced due to a saddle point when the current gradient is approximately zero [97] [98]. Here, the same hyperparameter setting is used in all experiments (before & after preprocessing). The ResNet50 network was proposed by the Microsoft research team [99], where 50 represented the number of deep layers. It contains 48-convolution, 1 average-pooling, and 1 max-pooling layer with a 224 x 224-input size. The residual block is a concatenation for three convolution layers. The overall architecture is shown in Fig. 5. The Inception-V2

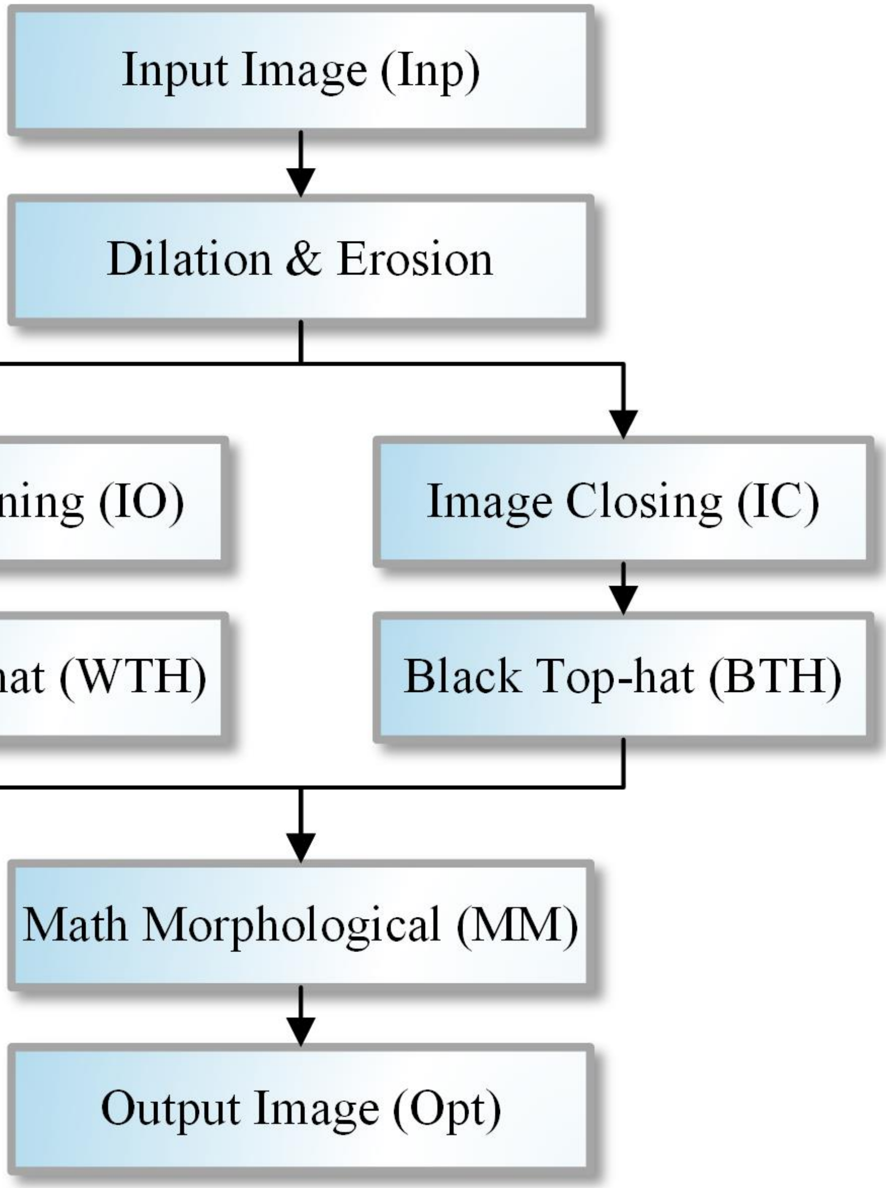

FIGURE 4: Mathematical morphological operation

ResNet network contains 148 deep layers, and it is capable of classifying 1000 classes. This network was developed by the Google research team. The network has an input-image size of 244 x 244, as shown in Fig. 5. A detailed description of the Inception-V2 ResNet, stem, and reduction blocks was discussed in [100]. The Inception V3 is a CNN developed by the Google research team. It contains 48 layers with an input-image size of 299 x 299. The Inception V3 network is trained using the ImageNet database, which contains one million training images in 1,000 categories. The Inception V3 has a decreased set of parameters due to factoring larger convolution layers into smaller ones and using different other means. A set of changes to the basic structure of the Inception V3 leads to a faster and more accurate architecture, which also works for smaller datasets as discussed in [101]. The RMSProp Optimizer is added to the Inception V3 network in addition to factorized 7x7 convolutions. The basic architecture of the Inception V3 network is presented in Fig. 6. The VGG19 is a CNN developed by the Visual Geometry Group at Oxford's and thus, the name VGG. The VGG19 is a variant of VGG models trained over the ImageNet database and contains 19 deep layers (16 convolution and 3 max-pooling layers) with an input-image size of 244 x 244. The kernel size used in the VGG19 is 3 x 3 with 1 stride size, whereas max-pooling is performed in a 2 x 2-pixel window with a stride size equal to 2. There are different variants of the VGG such as VGG16 and others. The major disadvantage of this CNN is its large size in terms of the number of

This article has been accepted for publication in a future issue of this journal, but has not been fully edited. Content may change prior to final publication. Citation information: DOI 10.1109/ACCESS.2021.3079204, IEEE Access

Algorithm 1 Data augmentation algorithm (DDA)

Input:
Benign B, Malignant M, Normal N segmented mammogram image.

Processing:
Step1: ∀ B, rotate to 0°, 90°, 180°, 270°
Step2: Perform flip on all step1.
Step3: ∀ M, rotate to 0°, 90°, 180°, 270°
Step4: Perform flip on all step3
Step5: ∀ N, rotate to 0°, 90°, 180°, 270°
Step6: Perform flip on all step5
Repeat for all training data

Output:
Save steps1,2,3,4,5,6

parameters to be trained. The VGG19 CNN is bigger than the VGG16. However, since the VGG19 performs almost as well as the VGG16, many people use the VGG16 [102]. The basic VGG19 architecture is presented in Fig. 6. The VGG16 is trained over the ImageNet database. Its architecture is deep and very simple. As shown in Fig. 6, it consists of 13 convolution layers and 5 max-pooling layers, followed by three FCLs and an SM classifier. The input is a 224 x 244-RGB image. The applied filters are 3 x 3 with a stride equal 1, whereas max-pooling is a 2 x 2-pixel window with a stride equal to 2 [102].

IV. RESULTS

A. DATASET DESCRIPTION

As shown in Fig. 7, the digital database for screening mammography (DDSM), MIAS, and private datasets are the most popular databases used for BC-classification models based on the statistics discussed on [103]. In this work, the applied mammogram database was provided by MIAS. Every image has a 1024 x 1024 size in portable gray map (PGM) format. The MIAS includes 322 images in three classes, 61 images for the benign case, 52 images for the malignant case, and 209 for the normal case. Data details are shown in Table 2. It provides details for ground-truth information on the mammogram images such as background tissue, abnormality present class, tumor type, abnormality center coordinates, and approximate radius for enclosing the abnormality circle. The abnormality class is presented by six forms; calcification (CALC), well-defined circumscribed masses (CIRC), spiculated masses (SPIC), other ill-defined masses (MISC), architectural distortion (ARCH), and asymmetry. A tumor region in the mammogram images is presented in Fig. 8.

B. EXPERIMENTAL ANALYSIS

In this section, several experiments conducted for investigating the performance of the proposed model on the MIAS dataset are presented. Here, TL is applied to five DL models (Inception V3, Inception-V2 ResNet, VGG16, VGG19, and ResNet50) and compared in terms of accuracy, precision, sensitivity, specificity, and AUC. The dataset was divided into three classes “Benign, Malignant, and Normal.” Then, it was split to 80% and 20% for the training and testing tasks, respectively. The efficiency of the proposed models was measured using the evaluation metrics for three classes, as shown in Table 3 and Eqs. 6 - 10. The benefits of preprocessing were investigated by conducting experiments twice, before and after preprocessing. The classifier performance results without preprocessing are presented in Table 4. It can be observed that the Inception-V2 ResNet achieves the best performance results in terms of accuracy, whereas the Inception V3 was ranked the second-best in terms of accuracy. On the other hand, the VGG16 achieves the best results in terms of sensitivity and specificity with 55.76%

TABLE 1: Parameter settings.

Sr. no	Parameter	Value
1	Minimum batch size	10
2	Maximum Epochs	20
3	Learn-rate drop factor	0.5
4	Initial-learn rate	1e-4
5	Learn-rate drop period	5

TABLE 2: MIAS data description.

Class	Sub-class of abnormality present	Number
Benign	CIRC	19
	CALC	10
	SPIC	11
	MISC	7
	ARCH	9
	ASYM	6
		Total = 62
Malignant	CIRC	4
	CALC	13
	SPIC	8
	MISC	7
	ARCH	10
	ASYM	9
		Total = 51
Normal	—	209

This article has been accepted for publication in a future issue of this journal, but has not been fully edited. Content may change prior to final publication. Citation information: DOI 10.1109/ACCESS.2021.3079204, IEEE Access

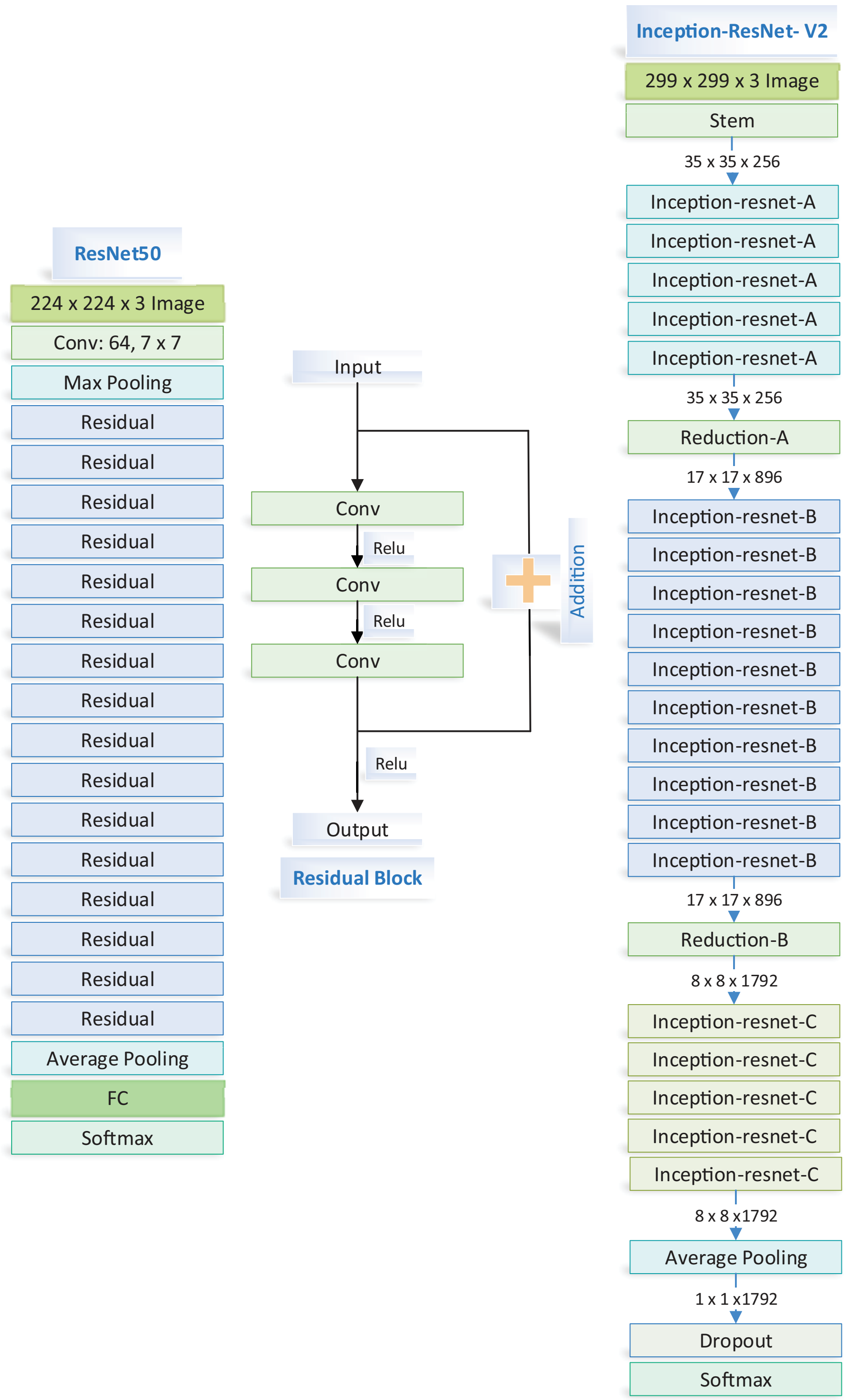

FIGURE 5: The ResNet50 and Inception V2-ResNet architectures

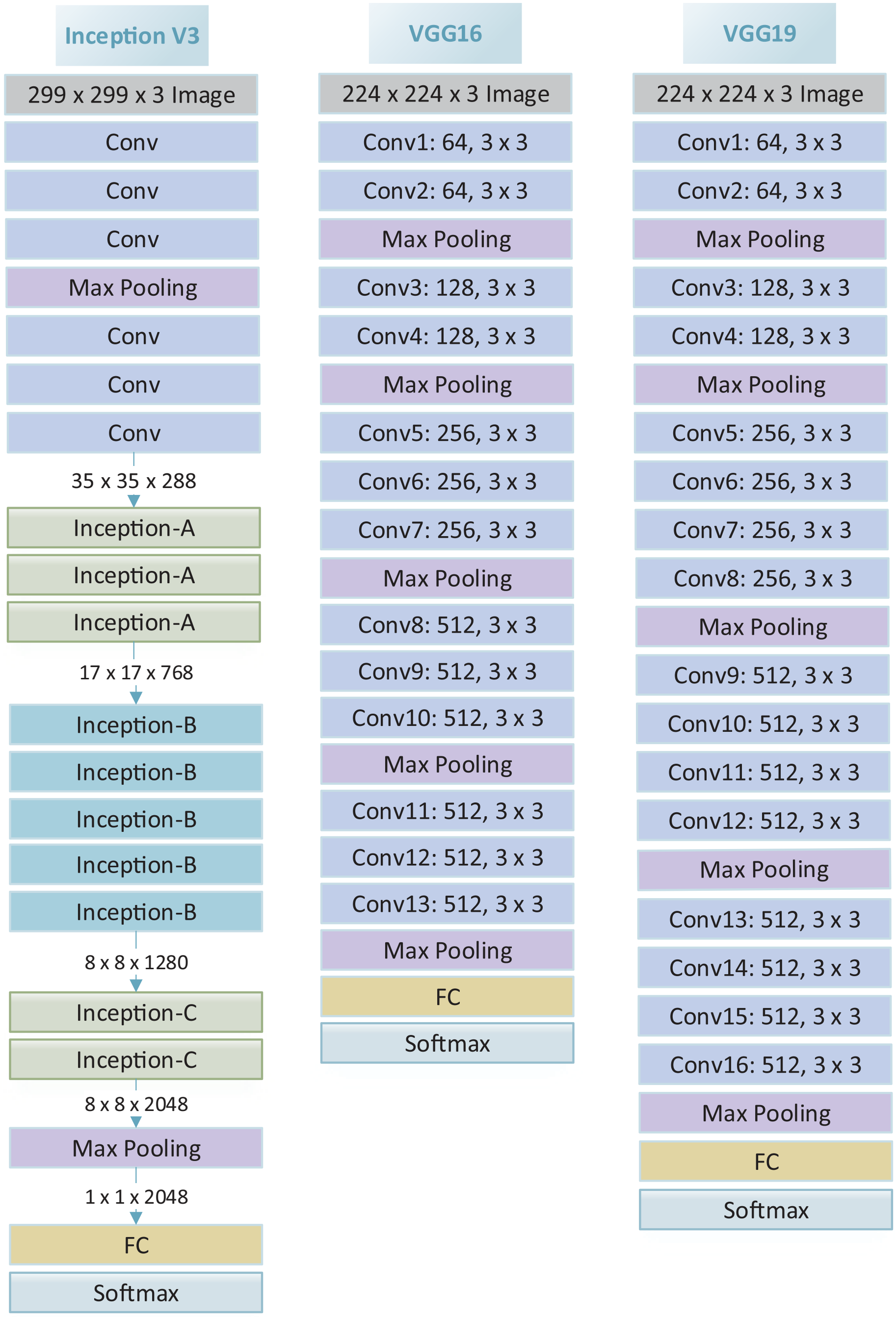

FIGURE 6: The Inception V3, VGG16, and VGG19 architectures

and 69.68%, respectively. Also, the ResNet50 achieves better results in terms of precision, AUC, and the F-score with values of 34.84%, 0.55, and 34.00%. The first component of the proposed model for preprocessing phase results is described in Fig. 9. The training data to be used as a training input for the proposed CNN are then augmented using DAA, as shown in Fig. 10. The results presented in Table 5 confirm that the VGG16 achieves the best results in the case of TL in the BC detection mechanism with SM classifier.

This article has been accepted for publication in a future issue of this journal, but has not been fully edited. Content may change prior to final publication. Citation information: DOI 10.1109/ACCESS.2021.3079204, IEEE Access

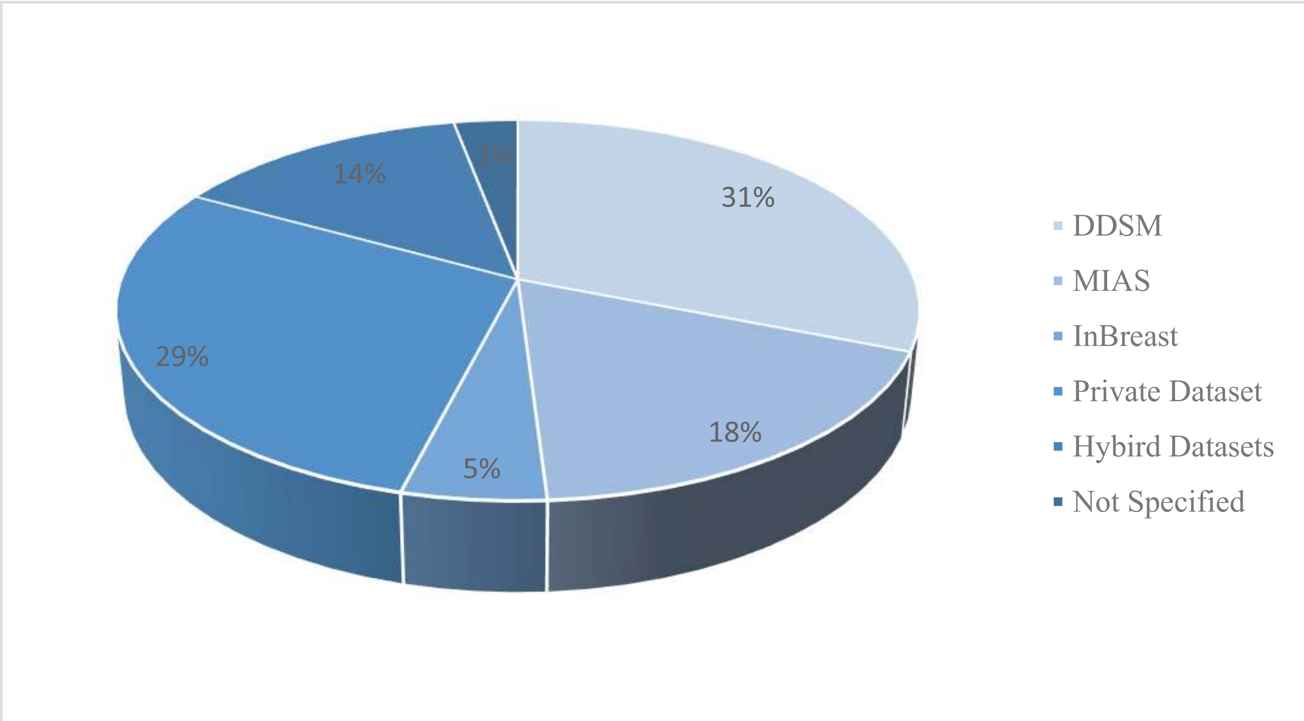

FIGURE 7: Dataset frequency usage for breast-tumor classification

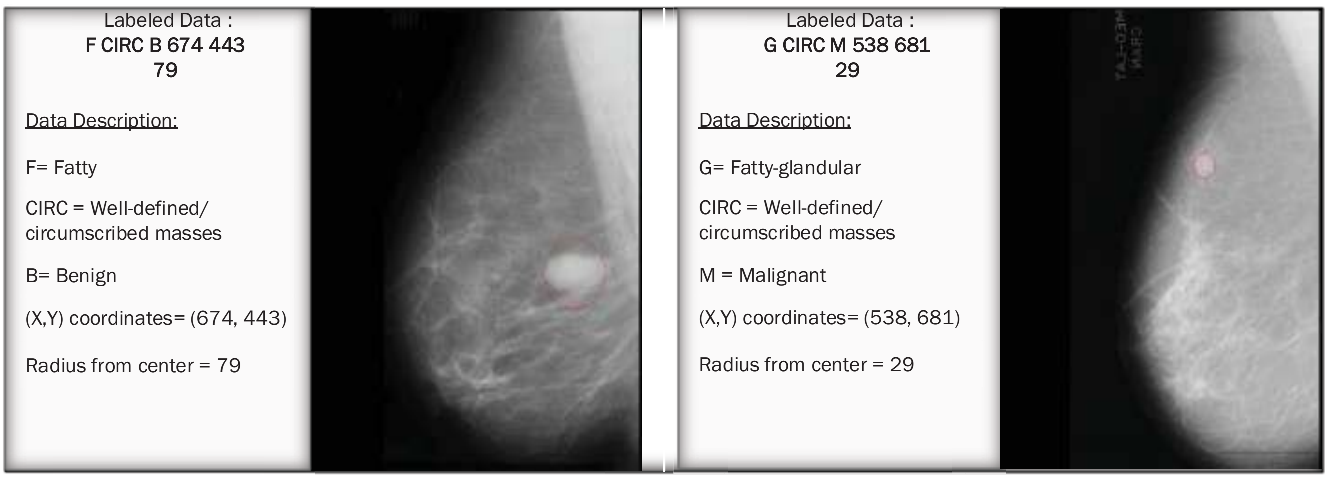

FIGURE 8: Tumor description in the mammogram images

TABLE 3: Evaluation metrics for BC-classification.

		Predict		
		Benign	Malignant	Normal
Actual	Benign	P_{BB} (TP)	P_{MB}	P_{NB}
	Malignant	P_{BM}	P_{MM} (TP)	P_{NM}
	Normal	P_{BN}	P_{MN}	P_{NN} (TP)

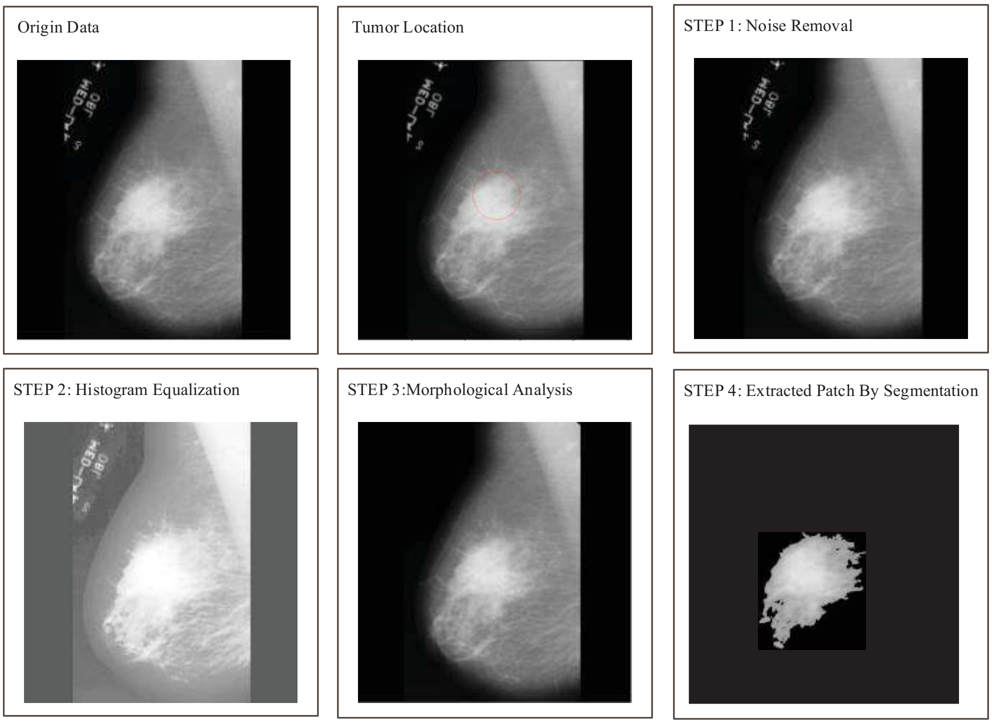

FIGURE 9: MIAS data preprocessing results

TABLE 4: BC-classification performance of various CNNs before preprocessing.

CNN	Classifier Performance					
	Accuracy (%)	Sensitivity (%)	Specificity (%)	Precision (%)	AUC	F-score (%)
Inception V3	62.50	33	63.7	33.8	0.43	29.70
VGG19	54.69	21.21	63.9	27.67	0.43	24.00
VGG16	59.38	55.76	69.68	32.1	0.49	30.30
ResNet50	54.69	34.77	66.62	34.84	0.55	34.00
Inception-V2 ResNet	64.06	0.22	55.12	32.5	0.51	26.00

$$\text{Accuracy} = \frac{P_{BB} + P_{MM} + P_{NN}}{P_{BB} + P_{MB} + P_{NB} + P_{BM} + P_{MM} + P_{NM} + P_{BN} + P_{MN} + P_{NN}} \tag{6}$$

$$\text{Sensitivity} = \frac{TP}{TP + FN} \tag{7}$$

$$\text{Precision} = \frac{TP}{TP + FP} \tag{8}$$

$$\text{Specificity} = \frac{TN}{TN + FP} \tag{9}$$

$$\text{F - score} = \frac{2 * \text{Percision} * \text{Sensitivity}}{Percision + Sensitivity} \tag{10}$$

This article has been accepted for publication in a future issue of this journal, but has not been fully edited. Content may change prior to final publication. Citation information: DOI 10.1109/ACCESS.2021.3079204, IEEE Access

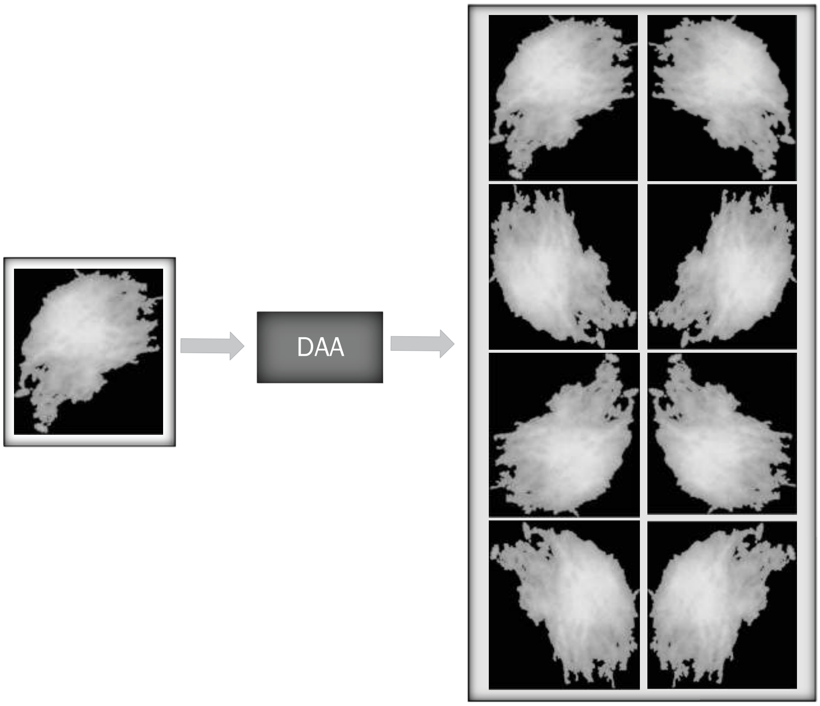

FIGURE 10: Results obtained using the data augmentation algorithm

TABLE 5: BC-classification performance of various CNNs after preprocessing using 80:20 and SM classifier.

CNN	Classifier Performance					
	Accuracy (%)	**Sensitivity (%)**	**Specificity (%)**	**Precision (%)**	**AUC**	**F-score (%)**
Inception V3	96.19	92.6	96.7	91.3	0.99	91.8
VGG19	94.35	89.86	94.8	88	0.97	88.3
VGG16	96.77	96	98	91	0.99	93
ResNet50	95.27	92	95.6	90	0.97	91
Inception-V2 ResNet	93.42	90.66	96	82.7	0.978	86

TABLE 6: BC-classification performance of various CNNs per class using 80:20 and SM classifier.

CNN	Class	Classifier performance per class					
		Accuracy (%)	**Sensitivity**	**Specificity**	**Precision**	**AUC**	**F-score**
Inception V3	Benign	96.89	0.96	0.97	0.87	0.99	0.91
	Malignant	96.02	0.86	0.98	0.89	0.98	0.874
	Normal	95.67	0.96	0.95	0.98	0.99	0.97
VGG19	Benign	94.12	0.80	0.982	0.93	0.96	0.86
	Malignant	95.5	0.946	0.956	0.76	0.986	0.84
	Normal	93.43	0.95	0.905	0.95	0.973	0.95
VGG16	Benign	97.06	0.99	0.97	0.85	0.992	0.914
	Malignant	97.4	0.95	0.98	0.88	0.99	0.91
	Normal	95.85	0.94	0.99	1.0	0.992	0.97
ResNet50	Benign	94.81	0.89	0.96	0.83	0.95	0.86
	Malignant	97.58	0.92	0.99	0.92	0.99	0.92
	Normal	93.43	0.94	0.92	0.96	0.97	0.95
Inception-V2 ResNet	Benign	92.21	0.89	0.93	0.67	0.965	0.764
	Malignant	96.02	0.93	0.97	0.82	0.988	0.87
	Normal	92.04	0.90	0.98	0.99	0.98	0.94

This article has been accepted for publication in a future issue of this journal, but has not been fully edited. Content may change prior to final publication. Citation information: DOI 10.1109/ACCESS.2021.3079204, IEEE Access

TABLE 7: BC-classification performance of various CNNs after preprocessing using 10-fold cross-validation and SM classifier.

CNN	Classifier Performance					
	Accuracy (%)	Sensitivity (%)	Specificity (%)	Precision (%)	AUC	F-score (%)
Inception V3	96.41	93.2	97.6	92.1	0.99	92.6
VGG19	94.44	90.62	93.22	89.02	0.98	89.81
VGG16	96.65	95.44	96.92	91.5	0.98	93.42
ResNet50	96.01	91.12	96.5	90.2	0.98	90.65
Inception-V2 ResNet	93.83	91.44	93.2	83.1	0.98	87.07

TABLE 8: BC-classification performance of various CNNs after preprocessing using 80:20 and SVM classifier.

CNN	Classifier Performance					
	Accuracy (%)	Sensitivity (%)	Specificity (%)	Precision (%)	AUC	F-score (%)
Inception V3	98.15	96.93	98.57	95.4	0.993	96
VGG19	95.84	91.33	96.37	90.66	0.982	91.33
VGG16	98.96	97.83	99.13	97.35	0.995	97.66
ResNet50	97.11	94.73	97.6	93.03	0.978	93.66
Inception-V2 ResNet	94.23	88	94.96	87.2	0.984	87.33

TABLE 9: BC-classification performance of various CNNs per class using 80:20 and SVM classifier.

CNN	Class	Classifier performance per class					
		Accuracy (%)	Sensitivity	Specificity	Precision	AUC	F-score
Inception V3	Benign	98.62	0.99	0.985	0.936	0.997	0.96
	Malignant	98.1	0.945	0.9876	0.934	0.99	0.94
	Normal	97.75	0.973	0.984	0.992	0.992	0.98
VGG19	Benign	95.67	0.889	0.972	0.881	0.971	0.89
	Malignant	96.19	0.888	0.975	0.869	0.99	0.88
	Normal	95.67	0.963	0.944	0.97	0.985	0.97
VGG16	Benign	99.31	0.99	0.993	0.97	0.997	0.98
	Malignant	98.62	0.956	0.991	0.956	0.992	0.96
	Normal	98.96	0.989	0.99	0.99	0.996	0.99
ResNet50	Benign	97.4	0.935	0.982	0.927	0.96	0.93
	Malignant	97.23	0.941	0.977	0.88	0.992	0.91
	Normal	96.71	0.966	0.969	0.984	0.982	0.97
Inception-V2 ResNet	Benign	94.12	0.872	0.955	0.809	0.975	0.84
	Malignant	94.64	0.821	0.971	0.847	0.99	0.83
	Normal	93.94	0.947	0.923	0.96	0.989	0.95

TABLE 10: BC-classification performance of various CNNs after preprocessing using 10-fold cross-validation and SVM classifier.

CNN	Classifier Performance					
	Accuracy (%)	Sensitivity (%)	Specificity (%)	Precision (%)	AUC	F-score (%)
Inception V3	98.45	97.2	98.9	93.5	0.994	95.31
VGG19	95.92	92.41	95.21	91.96	0.99	92.18
VGG16	98.87	97.27	98.2	98.84	0.993	98.04
ResNet50	96.87	94.24	96.99	95.45	0.97	94.84
Inception-V2 ResNet	94.76	88.86	94.72	88.14	0.987	88.49

TABLE 11: Comparison between the proposed model and existing models.

Method	Accuracy (%)	Sensitivity (%)	Specificity (%)	Precision (%)	AUC	F-score (%)
Abbas (2016)	91.5	92	84.2	-	0.91	-
Charan (2018)	65	-	-	-	-	-
Ting et al. (2019)	90.50	89.47	90.71	-	0.90	-
Sha et al. (2020)	92	96	93	-	-	-
Proposed	98.96	97.83	99.13	97.35	0.995	97.66

The detailed results per class are presented in Table 6. From this table, it can be observed that: 1) In the benign case, the VGG16 was ranked first in terms of accuracy, sensitivity, AUC, and the F-score, whereas the VGG19 was ranked first in terms of specificity and precision. 2) In the malignant case, the ResNet50 achieved the best accuracy, specificity, precision, and the F-score. In the last case (Normal), the VGG16 was ranked first in terms of accuracy, specificity, precision, and AUC, whereas the Inception V3 was ranked first in sensitivity.

The results of 10-fold cross-validation are shown in Table 7. It can be noted that the cross-validation method achieved better results than the 80-20 technique in all CNNs except VGG16. The results obtained from the SVM classifier achieved better than the results obtained from the SM classifier as presented in details in Tables 8 - 10. The experiments performed are presented in Table 11, where the performance is compared with four other existing models. The analysis results confirm that the proposed model performs better than other existing models in terms of accuracy, sensitivity, specificity, and AUC.

V. CONCLUSION

In this paper, a novel deep learning model for improving the classification results on the MIAS dataset was proposed. The purpose of this model is to help medical doctors in BC detection and diagnosis. The MIAS images were divided into three different classes, benign, malignant, and normal. The original MIAS dataset was pre-processed for noise removal, improving contrast in breast images, non-breast region removal, and determining the cancerous area. The data augmentation concept was also proposed for increasing the size of a dataset to enhance the performance of the CNN structure. Then, the freezing and fine-tuning strategies were used to improve the mass-lesion classification accuracy of the mentioned dataset. The VGG16 model achieved the best accuracy, sensitivity, specificity, AUC, and the F-score compared with four other models. Finally, it can be concluded that integrating the CNN using learning transfer in the screening mechanism, a clear improvement can be achieved compared with other existing approaches. The results showed 98.96% accuracy, 97.83% sensitivity, 99.13% specificity, 97.35% precision, 97.66% F-score, and 0.995 AUC. These results are better than the other mentioned methods.

In future work, the proposed method can be further used to diagnosis or prognosis of paraquat-poisoned patients [104]–[109], identification of poisoning status [110]–[112], diagnosis of tuberculous pleural effusion [113], differentiation of malignant and benign thyroid nodules [114], early diagnosis of Parkinson's disease [115]–[119], RNA secondary structure prediction [120], detection of erythemato-squamous diseases [121], online recognition of foreign fibers in cotton [122].

VI. ACKNOWLEDGEMENT

All authors have equally contributed to this work.

REFERENCES

[1] Lowry, Kathryn P., et al. "Long-term outcomes and cost-effectiveness of breast cancer screening with digital breast tomosynthesis in the United States." JNCI: Journal of the National Cancer Institute 112.6 (2020): 582-589.

[2] George, Sharon A. "Barriers To Breast Cancer Screening: An Integrative Review." Health Care for Women International, vol. 21, no. 1, 2000, pp. 53–65., doi:10.1080/073993300245401.

[3] Pamela Hallquist Viale, Rn, Ms, Cns, Anp. "The American Cancer Society's Facts & Figures: 2020 Edition." Journal of the Advanced Practitioner in Oncology, vol. 11, no. 2, 2020, doi:10.6004/jadpro.2020.11.2.1.

[4] Zhou, Juan, et al. "Weakly Supervised 3D Deep Learning for Breast Cancer Classification and Localization of the Lesions in MR Images." Journal of Magnetic Resonance Imaging, vol. 50, no. 4, 2019, pp. 1144–1151., doi:10.1002/jmri.26721.

[5] Soomro, B. A. and Lakhan, G. R. and Mangi, S. and Shah, N. "Predicting entrepreneurial intention among business students of public sector universities of Pakistan: an application of the entrepreneurial event mode." World Journal of Entrepreneurship, Management and Sustainable Development, vol. 16, no. 3, 2020, pp. 219-2301.

[6] Zhu, W. , et al. "Evaluation of Sino Foreign Cooperative Education Project Using Orthogonal Sine Cosine Optimized Kernel Extreme Learning Machine." IEEE Access PP.99(2020):1-1.

[7] Lin, A. , et al. "Predicting Intentions of Students for Master Programs using a Chaos-induced Sine Cosine-based Fuzzy K-Nearest Neighbor Classifier." IEEE Access PP.99(2019):1-1.

[8] J Tu, et al. "Predict the Entrepreneurial Intention of Fresh Graduate Students Based on an Adaptive Support Vector Machine Framework." Mathematical Problems in Engineering 2019(2019):1-16.

[9] Wei, Y. , et al. "An Improved Grey Wolf Optimization Strategy Enhanced SVM and Its Application in Predicting the Second Major." Mathematical Problems in Engineering,2017,(2017-02-20) 2017(2017):1-12.

[10] Yza, B , et al. "Towards Augmented Kernel Extreme Learning Models for Bankruptcy Prediction: Algorithmic Behavior and Comprehensive Analysis - ScienceDirect." Neurocomputing (2020).

[11] Yu , C. , et al. "SGOA: annealing-behaved grasshopper optimizer for global tasks." Engineering with Computers 2(2021):1-28.

[12] Cai, Z. , et al. "Evolving an optimal kernel extreme learning machine by using an enhanced grey wolf optimization strategy." Expert Systems with Applications 138(2019):112814-.

[13] Xu, Y. , et al. "An Efficient Chaotic Mutative Moth-flame-inspired Optimizer for Global Optimization Tasks." Expert Systems with Applications 129.SEP.(2019):135-155.

[14] Luo, J. , et al. "An Improved Grasshopper Optimization Algorithm with Application to Financial Stress Prediction." Applied Mathematical Modelling 64.DEC.(2018):654-668.

[15] D Zhao, et al. "An Effective Computational Model for Bankruptcy Prediction Using Kernel Extreme Learning Machine Approach." Computational Economics 49.2(2017):325-341.

[16] Wang, M. , et al. "Grey wolf optimization evolving kernel extreme learning machine: Application to bankruptcy prediction." Engineering Applications of Artificial Intelligence (2017).

[17] Wang, Lzt , et al. "Haze Concentration Adaptive Network for Image Dehazing." Neurocomputing 439.6(2021).

[18] Zhang, X. , et al. "Robust Feature Learning for Adversarial Defense via Hierarchical Feature Alignment." Information Sciences (2020).

[19] Huang, P. , et al. "Self-filtering image dehazing with self-supporting module." Neurocomputing (2020).

[20] Wang, T. , et al. "Video Deblurring via Spatiotemporal Pyramid Network and Adversarial Gradient Prior." Computer Vision and Image Understanding 203(2021):103135.

[21] Yan Caixia, Chang, Xiaojun, Luo Minnan, Zheng Qinghua, Zhang Xiaoqin, Li Zhihui, Nie Feiping. "Self-weighted Robust LDA for Multiclass Classification with Edge Classes SO ACM TRANSACTIONS ON INTELLIGENT SYSTEMS AND TECHNOLOGY." ACM Transactions on Intelligent Systems and Technology, 2020. 12(1): p. 1-19.

[22] Zhang, X., et al., Top-k feature selection framework using robust 0-1 integer programming. IEEE Transactions on Neural Networks and Learning Systems, 2020: p. DOI: 10.1109/TNNLS.2020.3009209.

[23] Zhang, X., et al., Pyramid channel-based feature attention network for image dehazing. Computer Vision and Image Understanding, 2020. 197: p. 103003.

[24] Zhang, X., et al., Attention-based interpolation network for video deblurring. Neurocomputing, 2020: p. DOI: 10.1016/j.neucom.2020.04.147.

This article has been accepted for publication in a future issue of this journal, but has not been fully edited. Content may change prior to final publication. Citation information: DOI 10.1109/ACCESS.2021.3079204, IEEE Access

[25] Liu, W., et al., Pair-based uncertainty and diversity promoting early active learning for person re-identification. ACM Transactions on Intelligent Systems and Technology, 2020. 11(2): p. 1-15.
[26] Zhang, X., et al., Multi-level Fusion and Attention-guided CNN for Image Dehazing. IEEE Transactions on Circuits and Systems for Video Technology, 2020: p. DOI: 10.1109/TCSVT.2020.3046625.
[27] Zhang, X., et al., Recursive neural network for video deblurring. IEEE Transactions on Circuits and Systems for Video Technology, 2020: p. DOI: 10.1109/TCSVT.2020.3035722.
[28] Zhang, X., et al., Robust low-rank tensor recovery with rectification and alignment. IEEE Transactions on Pattern Analysis and Machine Intelligence, 2019. 43(1): p. 238-255.
[29] Zhao, H., et al., Parallel and efficient approximate nearest patch matching for image editing applications. Neurocomputing, 2018. 305: p. 39-50.
[30] Zhao, Y., et al., Parallel style-aware image cloning for artworks. IEEE Transactions on Visualization and Computer Graphics, 2014. 21(2): p. 229-240.
[31] Yang, Y., et al., Semantic portrait color transfer with internet images. Multimedia Tools and Applications, 2017. 76(1): p. 523-541.
[32] Zhao, H.-L., et al., Structure-aware nonlocal optimization framework for image colorization. Journal of Computer Science and Technology, 2015. 30(3): p. 478-488.
[33] Zhao, H., et al., Real-time directional stylization of images and videos. Multimedia Tools and Applications, 2013. 63(3): p. 647-661.
[34] Lu, S., et al., Real-time image marbleization. Multimedia Tools and Applications, 2013. 64(3): p. 795-808.
[35] Lu, S., et al., Mathematical marbling. IEEE Computer Graphics and Applications, 2011. 32(6): p. 26-35.
[36] Zhao, H., et al., Efficient image decolorization with a multimodal contrast-preserving measure. Computers Graphics, 2018. 70: p. 251-260.
[37] Li, X., et al., Learning a convolutional neural network for propagation-based stereo image segmentation. The Visual Computer, 2020. 36(1): p. 39-52.
[38] Li, X., et al., Interactive image recoloring by combining global and local optimization. Multimedia Tools and Applications, 2016. 75(11): p. 6431-6443.
[39] Huang, H., et al., Manifold-preserving image colorization with nonlocal estimation. Multimedia Tools and Applications, 2015. 74(18): p. 7555-7568.
[40] Gu, N., et al., Efficient sequential feature selection based on adaptive eigenspace model. Neurocomputing 2015. 161: p. 199-209.
[41] Zhou, P., et al., Unsupervised feature selection for balanced clustering. Knowledge-Based Systems, 2020. 193: p. 105417.
[42] Fan, M., et al., Dimensionality reduction: An interpretation from manifold regularization perspective. Information Sciences, 2014. 277: p. 694-714.
[43] Fan, M., et al., Efficient isometric multi-manifold learning based on the self-organizing method. Information Sciences, 2016. 345: p. 325-339.
[44] Yang, C., et al., Superpixel-based unsupervised band selection for classification of hyperspectral images. IEEE Transactions on Geoscience and Remote Sensing, 2018. 56(12): p. 7230-7245.
[45] Wang, S., et al., Convolutional neural network-based hidden Markov models for rolling element bearing fault identification. Knowledge-Based Systems, 2018. 144: p. 65-76.
[46] Wang, S. and J. Xiang, A minimum entropy deconvolution-enhanced convolutional neural networks for fault diagnosis of axial piston pumps. Soft Computing, 2020. 24(4): p. 2983-2997.
[47] Gao, Q., et al., A multi-sensor fault detection strategy for axial piston pump using the Walsh transform method. International Journal of Distributed Sensor Networks, 2018. 14(4): p. 1550147718772531.
[48] Song, W., J. Xiang, and Y. Zhong, A simulation model based fault diagnosis method for bearings. Journal of Intelligent Fuzzy Systems, 2018. 34(6): p. 3857-3867.
[49] Liu, X., H. Huang, and J. Xiang, A personalized diagnosis method to detect faults in gears using numerical simulation and extreme learning machine. Knowledge-Based Systems, 2020. 195: p. 105653.
[50] Yu, H., et al., Improved Butterfly Optimizer-Configured Extreme Learning Machine for Fault Diagnosis. Complexity, 2021. 2021: p. 6315010.
[51] Wang, S.J., et al., Face recognition and micro-expression recognition based on discriminant tensor subspace analysis plus extreme learning machine. Neural Processing Letters, 2014. 39(1): p. 25-43.
[52] Wang, S.J., et al., Sparse tensor canonical correlation analysis for micro-expression recognition. Neurocomputing, 2016. 214: p. 218-232.
[53] Liu, Y.J., et al., A Main Directional Mean Optical Flow Feature for Spontaneous Micro-Expression Recognition. Ieee Transactions on Affective Computing, 2016. 7(4): p. 299-310.
[54] Yan, W.J. and Y.H. Chen, Measuring dynamic micro-expressions via feature extraction methods. Journal of Computational Science, 2018. 25: p. 318-326.
[55] Qu, F.B., et al., CAS(ME)(2): A Database for Spontaneous Macro-Expression and Micro-Expression Spotting and Recognition. Ieee Transactions on Affective Computing, 2018. 9(4): p. 424-436.
[56] Wang, Y., et al., Effective recognition of facial micro-expressions with video motion magnification. Multimedia Tools and Applications, 2017. 76(20): p. 21665-21690.
[57] Wang, S.-J., et al., MESNet: A Convolutional Neural Network for Spotting Multi-Scale Micro-Expression Intervals in Long Videos. IEEE Transactions on Image Processing, 2021.
[58] Wang, D., et al., A content-based recommender system for computer science publications. Knowledge-Based Systems, 2018. 157: p. 1-9.
[59] Guan, R., et al., Deep Feature-Based Text Clustering and Its Explanation. IEEE Transactions on Knowledge and Data Engineering, 2020: p. 1-1.
[60] Feng, C., et al., Prediction of trust propensity from intrinsic brain morphology and functional connectome. Human Brain Mapping, 2021. 42(1): p. 175-191.
[61] Wang, H., X. Wu, and L.J.I.T.o.A.C. Yao, Identifying cortical brain directed connectivity networks from high-density EEG for emotion recognition. IEEE Transactions on Affective Computing, 2020: p. DOI: 10.1109/TAFFC.2020.3006847.
[62] Zhang, H., et al., Altered Time-Frequency Feature in Default Mode Network of Autism Based on Improved Hilbert-Huang Transform. IEEE Journal of Biomedical and Health Informatics, 2020: p. DOI: 10.1109/JBHI.2020.2993109.
[63] Li, Z., et al., The Recognition of Multiple Anxiety Levels Based on Electroencephalograph. IEEE Transactions on Affective Computing, 2019: p. DOI: 10.1109/TAFFC.2019.2936198.
[64] Yao, Z., et al., Morphological changes in subregions of hippocampus and amygdala in major depressive disorder patients. Brain Imaging and Behavior, 2020. 14(3): p. 653-667.
[65] Fei, X., et al., Projective parameter transfer based sparse multiple empirical kernel learning Machine for diagnosis of brain disease. Neurocomputing, 2020. 413: p. 271-283.
[66] Li, Y., et al., Epileptic seizure detection in EEG signals using sparse multiscale radial basis function networks and the Fisher vector approach. Knowledge-Based Systems, 2019. 164: p. 96-106.
[67] Chen, H., et al., Using blood indexes to predict overweight statuses: an extreme learning machine-based approach. PloS one, 2015. 10(11): p. e0143003.
[68] Sun, X., et al., Selection of interdependent genes via dynamic relevance analysis for cancer diagnosis. Journal of Biomedical Informatics, 2013. 46(2): p. 252-258.
[69] Wang, M. and H. Chen, Chaotic multi-swarm whale optimizer boosted support vector machine for medical diagnosis. Applied Soft Computing, 2020. 88: p. 105946.
[70] Wang, M., et al., Toward an optimal kernel extreme learning machine using a chaotic moth-flame optimization strategy with applications in medical diagnoses. Neurocomputing, 2017. 267: p. 69-84.
[71] Shen, L., et al., Evolving support vector machines using fruit fly optimization for medical data classification. Knowledge-Based Systems, 2016. 96: p. 61-75.
[72] Liu, D., et al., Medical image classification using spatial adjacent histogram based on adaptive local binary patterns. Computers in Biology and Medicine, 2016. 72: p. 185-200.
[73] Shan, W., et al., Double adaptive weights for stabilization of moth flame optimizer: Balance analysis, engineering cases, and medical diagnosis. Knowledge-Based Systems, 2020: p. 106728.
[74] Zhao, H., et al., High-quality retinal vessel segmentation using generative adversarial network with a large receptive field. International Journal of Imaging Systems and Technology, 2020. 30(3): p. 828-842.
[75] Lotter, William, et al. "Robust breast cancer detection in mammography and digital breast tomosynthesis using annotation-efficient deep learning approach." arXiv preprint arXiv:1912.11027 (2019).
[76] Zhang, Qingchen, et al. "A survey on deep learning for big data." Information Fusion 42 (2018): 146-157.
[77] Saber, Abeer, et al. “Big-Data Aggregating, Linking, Integrating and Representing Using Semantic Web Technologies.” The International Conference on Advanced Machine Learning Technologies and Applications

(AMLTA2018) Advances in Intelligent Systems and Computing, 2018, pp. 331–342., doi:10.1007/978-3-319-74690-6_33.

[78] Weiss, Karl, et al. “A Survey of Transfer Learning.” Journal of Big Data, vol. 3, no. 1, 2016, doi:10.1186/s40537-016-0043-6.

[79] Samala, Ravi K, et al. “Multi-Task Transfer Learning Deep Convolutional Neural Network: Application to Computer-Aided Diagnosis of Breast Cancer on Mammograms.” Physics in Medicine & Biology, vol. 62, no. 23, 2017, pp. 8894–8908., doi:10.1088/1361-6560/aa93d4.

[80] Ting, Fung Fung, Yen Jun Tan, and Kok Swee Sim. "Convolutional neural network improvement for breast cancer classification." Expert Systems with Applications 120 (2019): 103-115.

[81] Toğaçar, Mesut, et al. “BreastNet: A Novel Convolutional Neural Network Model through Histopathological Images for the Diagnosis of Breast Cancer.” Physica A: Statistical Mechanics and Its Applications, vol. 545, 2020, p. 123592., doi:10.1016/j.physa.2019.123592.

[82] Abbas, Qaisar. “DeepCAD: A Computer-Aided Diagnosis System for Mammographic Masses Using Deep Invariant Features.” Computers, vol. 5, no. 4, 2016, p. 28., doi:10.3390/computers5040028.

[83] Sha, Zijun, et al. “Deep Learning and Optimization Algorithms for Automatic Breast Cancer Detection.” International Journal of Imaging Systems and Technology, vol. 30, no. 2, 2020, pp. 495–506., doi:10.1002/ima.22400.

[84] Charan, Saira, et al. “Breast Cancer Detection in Mammograms Using Convolutional Neural Network.” 2018 International Conference on Computing, Mathematics and Engineering Technologies (ICoMET), 2018, doi:10.1109/icomet.2018.8346384.

[85] Wahab, Noorul, et al. “Transfer Learning Based Deep CNN for Segmentation and Detection of Mitoses in Breast Cancer Histopathological Images.” Microscopy, vol. 68, no. 3, 2019, pp. 216–233., doi:10.1093/jmicro/dfz002.

[86] Jiang, Fan, et al. “Breast Mass Lesion Classification in Mammograms by Transfer Learning.” Proceedings of the 5th International Conference on Bioinformatics and Computational Biology - ICBCB 17, 2017, doi:10.1145/3035012.3035022.

[87] Khan, Sanaullah, et al. “A Novel Deep Learning Based Framework for the Detection and Classification of Breast Cancer Using Transfer Learning.” Pattern Recognition Letters, vol. 125, 2019, pp. 1–6., doi:10.1016/j.patrec.2019.03.022.

[88] Cao, Hongliu, et al. “Improve the Performance of Transfer Learning Without Fine-Tuning Using Dissimilarity-Based Multi-View Learning for Breast Cancer Histology Images.” Lecture Notes in Computer Science Image Analysis and Recognition, 2018, pp. 779–787., doi:10.1007/978-3-319-93000-8_88.

[89] Deniz, Erkan, et al. “Transfer Learning Based Histopathologic Image Classification for Breast Cancer Detection.” Health Information Science and Systems, vol. 6, no. 1, 2018, doi:10.1007/s13755-018-0057-x.

[90] Celik, Yusuf, et al. “Automated Invasive Ductal Carcinoma Detection Based Using Deep Transfer Learning with Whole-Slide Images.” Pattern Recognition Letters, vol. 133, 2020, pp. 232–239., doi:10.1016/j.patrec.2020.03.011.

[91] Said, Khairul Anuar Mat, and Asral Bahari Jambek. “A Study on Image Processing Using Mathematical Morphological.” 2016 3rd International Conference on Electronic Design (ICED), 2016, doi:10.1109/iced.2016.7804697.

[92] Wang, D., Khosla, A., Gargeya, R., Irshad, H., & Beck, A. H. (2016). Deep learning for identifying metastatic breast cancer. arXiv preprint arXiv:1606.05718.

[93] M. Sakr, A. Saber, O.M. Abo-Seida and A. Keshk, “Machine learning for breast cancer classification using k-star algorithm,” Applied Mathematics and Information Sciences journal, vol. 14, no. 5, pp. 855- 863, 2020.

[94] Hussien, A. G., Amin, M., Wang, M., Liang, G., Alsanad, A., Gumaei, A., & Chen, H. (2020). Crow search algorithm: theory, recent advances, and applications. IEEE Access, 8, 173548-173565.

[95] Nguyen, Quang Hung, et al. "Influence of Data Splitting on Performance of Machine Learning Models in Prediction of Shear Strength of Soil." Mathematical Problems in Engineering 2021 (2021).

[96] Kohavi, R. (1995, August). “A study of cross-validation and bootstrap for accuracy estimation and model selection”. In Ijcai (Vol. 14, No. 2, pp. 1137-1145).

[97] Qian, Ning. "On the momentum term in gradient descent learning algorithms." Neural networks 12.1 (1999): 145-151.

[98] Sutskever, I., Martens, J., Dahl, G., Hinton, G. (2013, February). On the importance of initialization and momentum in deep learning. In International conference on machine learning (pp. 1139-1147).

[99] He, Kaiming, et al. “Deep Residual Learning for Image Recognition.” 2016 IEEE Conference on Computer Vision and Pattern Recognition (CVPR), 2016, doi:10.1109/cvpr.2016.90.

[100] Szegedy, Christian, et al. "Inception-v4, inception-resnet and the impact of residual connections on learning." Thirty-first AAAI conference on artificial intelligence. 2017.

[101] Szegedy, Christian, et al. “Rethinking the Inception Architecture for Computer Vision.” 2016 IEEE Conference on Computer Vision and Pattern Recognition (CVPR), 2016, doi:10.1109/cvpr.2016.308.

[102] Simonyan, Karen, and Andrew Zisserman. "Very deep convolutional networks for large-scale image recognition." arXiv preprint arXiv:1409.1556 (2014).

[103] Tasdemir, Sena B. Yengec, et al. “A Review of Mammographic Region of Interest Classification.” WIREs Data Mining and Knowledge Discovery, 2020, doi:10.1002/widm.1357.

[104] Zhao, X., et al., "Chaos enhanced grey wolf optimization wrapped ELM for diagnosis of paraquat-poisoned patients. Computational Biology and Chemistry," 2019. 78: p. 481-490.

[105] Lufeng Hu, G.H., Jianshe Ma, Xianqin Wang, Huiling Chen, An Efficient Machine Learning Approach for Diagnosis of Paraquat-Poisoned Patients. Computers in Biology and Medicine, 2015. 59: p. 116-124.

[106] Hu, L., et al., A new machine-learning method to prognosticate paraquat poisoned patients by combining coagulation, liver, and kidney indices. Plos One, 2017. 12(10): p. e0186427.

[107] Hu, L., et al., An intelligent prognostic system for analyzing patients with paraquat poisoning using arterial blood gas indexes. Journal of Pharmacological and Toxicological Methods, 2017. 84: p. 78-85.

[108] Chen, H., et al., An Effective Machine Learning Approach for Prognosis of Paraquat Poisoning Patients Using Blood Routine Indexes. Basic Clinical Pharmacology Toxicology, 2017. 120(1): p. 86-96.

[109] Wen, C., et al., Metabolomics Analysis in Acute Paraquat Poisoning Patients Based on UPLC-Q-TOF-MS and Machine Learning Approach. Chemical Research in Toxicology, 2019. 32(4): p. 629-637.

[110] Zhu, J., et al., An Effective Machine Learning Approach for Identifying the Glyphosate Poisoning Status in Rats Using Blood Routine Test. IEEE Access, 2018. 6: p. 15653-15662.

[111] Zhu, J., et al., A New Evolutionary Machine Learning Approach for Identifying Pyrene Induced Hepatotoxicity and Renal Dysfunction in Rats. Ieee Access, 2019. 7: p. 15320-15329.

[112] Xu, Y., et al., A New Hybrid Machine Learning Approach for Prediction of Phenanthrene Toxicity on Mice. IEEE Access, 2019. 7: p. 138461-138472.

[113] Li, C., et al., Developing a new intelligent system for the diagnosis of tuberculous pleural effusion. Computer Methods and Programs in Biomedicine, 2018. 153: p. 211-225.

[114] Xia, J., et al., Ultrasound-based differentiation of malignant and benign thyroid Nodules: An extreme learning machine approach. Computer Methods and Programs in Biomedicine, 2017. 147: p. 37-49.

[115] Chen, H.-L., et al., An efficient hybrid kernel extreme learning machine approach for early diagnosis of Parkinson’s disease. Neurocomputing, 2016. 184: p. 131-144.

[116] Zuo, W.-L., et al., Effective detection of Parkinson’s disease using an adaptive fuzzy k-nearest neighbor approach. Biomedical Signal Processing and Control, 2013. 8(4): p. 364-373.

[117] Chen, H.-L., et al., An efficient diagnosis system for detection of Parkinson’s disease using fuzzy k-nearest neighbor approach. Expert Systems with Applications, 2013. 40(1): p. 263-271.

[118] Cai, Z., J. Gu, and H.-L. Chen, A New Hybrid Intelligent Framework for Predicting Parkinson’s Disease. Ieee Access, 2017. 5: p. 17188-17200.

[119] Cai, Z., et al., An Intelligent Parkinson’s Disease Diagnostic System Based on a Chaotic Bacterial Foraging Optimization Enhanced Fuzzy KNN Approach. Computational and Mathematical Methods in Medicine, 2018. 2018: p. 2396952.

[120] Wang, G., et al., A Novel Framework Based on ACO and PSO for RNA Secondary Structure Prediction. Mathematical Problems in Engineering, 2013. 2013: p. 796304.

[121] Liu, T., et al., A fast approach for detection of erythemato-squamous diseases based on extreme learning machine with maximum relevance minimum redundancy feature selection. International Journal of Systems Science, 2015. 46(5): p. 919-931.

[122] Zhao, X., et al., An Efficient and Effective Automatic Recognition System for Online Recognition of Foreign Fibers in Cotton. Ieee Access, 2016. 4: p. 8465-8475.

ABEER SABER was born in Damietta, Domyat, Egypt, in 1992. She received the B.Sc. Degree in Computer Science and the M.Sc. Degree in Computer Science from Mansoura University, Egypt, in 2013 and 2018, respectively. She is currently an Assistant Lecturer in Computer Science with the Faculty of Computers and Information, Kafr El-Sheikh University, Egypt. She has published many research articles in prestigious international conferences and reputable journals. Her current research interests include big data analysis, semantic web, linked open data, data mining, and machine learning.

MOHAMED SAKR was born in Shebin El-Kom, Menoufia, Egypt, in 1990. He received the B.Sc. degree in computer science, the M.Sc. degree in computer science, and the Ph.D. in computer science from Menoufia University, Egypt, in 2011, 2014,and 2019, respectively . He is currently a Lecturer of computer science with the Faculty of Computers and Information, Menoufia University. He has published many research articles published in prestigious international conferences and reputable journals. His current research interests include big data analysis, anomaly detection, data mining, and machine learning.

OSAMA M. ABO-SEIDA was born in Kotor, Tanta, Egypt, in 1968. He received the B.Sc. degree in mathematics, the M.Sc. degree in mathematics, and the Ph.D. from Tanta University, Egypt, in 1990 ,1994, and 1997, respectively. He is currently a Professor of mathematics and the Dean of the faculty of Computers and Information with Kafr El-Sheikh University. He has authored or coauthored many articles in international repute journals. His research interests include Wave Propagation, Applied Mathematics, Computional Electromagnetics, and Magnetical Networks.

ARABI E. KESHK received the B.Sc. in Electronic Engineering and M.Sc. in Computer Science and Engineering from Menoufia University, Faculty of Electronic Engineering in 1987 and 1995, respectively and received his PhD in Electronic Engineering from Osaka University, Japan in 2001. His research interest includes software testing, software engineering, distributed system, cloud computing, machine learning, IoT, big Data analytics, and bioinformatics.

HUILING CHEN is currently an associate professor in the college of computer science and artificial intelligence at Wenzhou University, China. He received his Ph.D. degree in department of computer science and technology at Jilin University, China. His present research interests center on machine learning and data mining, as well as their applications to medical diagnosis and bankruptcy prediction. He is currently serving as an associate editor of IEEE ACCESS. He is also a reviewer for many journals such as Applied Soft Computing, Artificial Intelligence in Medicine, Knowledge-based Systems, Future Generation Computer System. He has published more than 100 papers in international journals and conference proceedings, including Information Sciences, Pattern Recognition, Future Generation Computer System, Expert Systems with Applications, Knowledge-based Systems, Neurocomputing, PAKDD, and among others.